“On-The-Fly” Synthesis of Self-Supported LDH Hollow Structures Through Controlled Microfluidic Reaction-Diffusion Conditions

Author(s):
Mattera, Michele; Sorrenti, Alessandro; De Gregorio Perpiñá, Lidia; Oestreicher, Victor; Sevim, Semih; Arteaga, Oriol; Chen, Xiang-Zhong; Pané, Salvador; Abellán, Gonzalo; Puigmartí-Luis, Josep

Publication date:
2024-05-16

Permanent link:
https://doi.org/10.3929/ethz-b-000649795

Originally published in:
Small 20(20), https://doi.org/10.1002/smll.202307621

Funding acknowledgement:
181988 - Functional 2D porous crystalline materials (2DMats) (SNF)
206033 - Magnetically driven soft continuum robot-enabled localized prodrug delivery for cancer chemoimmunotherapy (SNF)
101047081/22.00021 - Magnetoelectric 3D printing technology - the revolution of actuatable composites (SBFI)

RESEARCH ARTICLE

NANO · MICRO small
www.small-journal.com

"On-The-Fly" Synthesis of Self-Supported LDH Hollow Structures Through Controlled Microfluidic Reaction-Diffusion Conditions

Michele Mattera, Alessandro Sorrenti, Lidia De Gregorio Perpiñá, Víctor Oestreicher, Semih Sevim, Oriol Arteaga, Xiang-Zhong Chen, Salvador Pané, Gonzalo Abellán, and Josep Puigmartí-Luis**

Layered double hydroxides (LDHs) are a class of functional materials that exhibit exceptional properties for diverse applications in areas such as heterogeneous catalysis, energy storage and conversion, and bio-medical applications, among others. Efforts have been devoted to produce millimeter-scale LDH structures for direct integration into functional devices. However, the controlled synthesis of self-supported continuous LDH materials with hierarchical structuring up to the millimeter scale through a straightforward one-pot reaction method remains unaddressed. Herein, it is shown that millimeter-scale self-supported LDH structures can be produced by means of a continuous flow microfluidic device in a rapid and reproducible one-pot process. Additionally, the microfluidic approach not only allows for an "on-the-fly" formation of unprecedented LDH composite structures, but also for the seamless integration of millimeter-scale LDH structures into functional devices. This method holds the potential to unlock the integrability of these materials, maintaining their performance and functionality, while diverging from conventional techniques like pelletization and densification that often compromise these aspects. This strategy will enable exciting advancements in LDH performance and functionality.

1. Introduction

Layered double hydroxides (LDHs), also referred to as anionic clays, are a sort of lamellar materials exhibiting a highly tunable chemical composition.[1] Their chemical structure consists of infinite sheets comprising octahedral divalent (M(II)) and trivalent cations (M(III)) connected through OH^- bridges.[2,3] These positively charged layers assemble through the inclusion of an (in)organic anion within their interlayer spaces. This arrangement gives rise to a plethora of inorganic as well as inorganic–organic hybrid materials with great potential in diverse application areas such as heterogeneous catalysis, energy storage, and conversion, and biomedical applications, among others.[4–7]

Over the last decades, significant efforts have been dedicated to unraveling the structure-property relationship of LDHs.[8] Researchers have focused on investigating

M. Mattera, L. De Gregorio Perpiñá, J. Puigmartí-Luis
Departament de Ciència dels Materials i Química Física
Institut de Química Teòrica i Computacional
University of Barcelona (UB)
Barcelona 08028, Spain
E-mail: josep.puigmarti@ub.edu

A. Sorrenti
Departament de Química Inorgànica i Orgànica (Secció de Química Orgànica)
University of Barcelona (UB)
Barcelona 08028, Spain

V. Oestreicher, G. Abellán
Institute of Molecular Science
University of Valencia (UVEG)
c/Catedrático José Beltrán 2, Paterna 46980, Spain
E-mail: gonzalo.abellan@uv.es

S. Sevim, S. Pané
Institute of Robotics and Intelligent Systems
ETH Zurich
Tannenstrasse 3, Zurich CH 8092, Switzerland

O. Arteaga
Departament de Fisica Aplicada
PLAT group
Universitat de Barcelona
IN2UB, Barcelona 08028, Spain

X.-Z. Chen
Institute of Optoelectronics
State Key Laboratory of Photovoltaic Science and Technology
Shanghai Frontiers Science Research Base of Intelligent Optoelectronics and Perception
Fudan University
Shanghai 200438, P. R. China

The ORCID identification number(s) for the author(s) of this article can be found under https://doi.org/10.1002/smll.202307621

DOI: 10.1002/smll.202307621

various factors that influence the properties of LDHs, including the M(II)/M(III) molar ratio,[9] the nature of the interlayer anion,[10] and/or the pH conditions employed during synthesis.[11] By carefully adjusting synthetic parameters, researchers have successfully demonstrated the ability to control the interlayer spacing, the charge density, and hence, the reactivity of LDHs.[12] Indeed, this trial-and-error optimization procedure has also enabled the customization of LDHs with specific functionalities, including enhanced catalytic activity,[13] controlled drug delivery,[14] and tailored adsorption and release properties.[15]

Research efforts have been also dedicated to exerting precise control over the nucleation, growth, crystal size and shape of LDHs.[5] This next level of control, spanning from the nanometer to the millimeter scale, is recognized as a critical parameter to enable the direct integration of these materials into ready-to-use functional devices. Significant advancements have been made in structuring LDHs, encompassing the fabrication of micrometric powders of porous nanoparticles,[16] as well as micro-structured millimeter-scale monoliths.[17] However, these achievements have been accomplished through multi-step and complex protocols including sol-gel techniques assisted by soft-templating methods,[18,19] and/or supported synthesis on diverse 2D or 3D solid supports, either through in situ coprecipitation or self-assembly of preformed LDH nanoparticles at the surface.[20] Despite the significant efforts toward the realization of millimeter-scale LDH structures, the preparation of self-supported LDH materials with controlled hierarchical structuring up to the millimeter scale using a straightforward one-pot reaction method remains unaddressed.

Microfluidic technologies are emerging as a powerful toolkit in the field of materials science, offering precise control over the growth mechanisms of functional materials, i.e., over crystallization processes and self-assembly pathways.[21] Additionally, these technologies enable efficient processing and shaping of materials into various morphologies, providing new avenues for materials design and development. In particular, planar (i.e., 2D) continuous flow microfluidic devices operating under laminar flow conditions have proved to provide an exquisite spatiotemporal control over reaction-diffusion (RD) processes and reactant concentration gradients (with constant mass transfer of reactants to the RD area), as the mixing between the chemical species dissolved in co-flowing streams occurs solely through molecular diffusion. Note that in a planar continuous flow microfluidic device this diffusion process takes place at the vertical liquid–liquid interface formed within the microfluidic channel, where the two co-flowing reagent-laden fluid streams interact.[22] This configuration of the RD area allows for the creation of a distinct synthetic environment that is dramatically different from those encountered in conventional bulk synthetic methods, where chaotic turbulent mixing is employed to achieve a fast and perfect homogenization of the reactants, at the expense of losing control over the RD phenomena.[21] For example, our previous research has shown that the utilization of the advanced spatiotemporal mixing achieved with a planar continuous flow microfluidic device enables control over the internal structure of a conductive supramolecular polymer. This level of control is typically unattainable using conventional synthetic approaches, which rely on turbulent mixing conditions, unless different molecular building blocks are employed.[23] Additionally, the RD conditions achieved at the vertical liquid-liquid interface, generated within the main channel height in planar continuous flow microfluidic devices, have also facilitated the precise control over morphogenesis during the microfluidic synthesis of a coordination polymer, allowing for the isolation of non-equilibrium intermediates.[24] The utilization of the same planar microfluidic device played also a crucial role in determining the degree of defects within the crystal structure of a spin-crossover material, thus also influencing its spin transition behavior.[25] Additionally, served as a pivotal tool in unveiling unprecedented growth pathways during the synthesis of a metal-organic framework (MOF).[26] In addition to enabling the controlled synthesis of different functional materials, the planar continuous flow microfluidic devices used in the aforementioned studies have also allowed for the direct printing of those materials, which otherwise are challenging to process using conventional bulk solvothermal methods, such as covalent organic frameworks (COFs).[27]

Herein, we demonstrate, for the first time, the utilization of a continuous flow microfluidic device for the controlled synthesis of millimeter-scale self-supported LDH hollow structures in a rapid (ca. 2 s) and reproducible one-pot reaction process. We introduce a different fluid stream configuration where the liquid–liquid interface has been transformed from a vertical arrangement to a concentric one employing a 3D hydrodynamic flow focusing set-up. This re-shaping of the liquid–liquid interface enables the expansion of the RD area beyond the limited height of the microfluidic channel typically found in planar continuous flow microfluidic devices. As a result, our findings conclusively demonstrate that the utilization of this concentric liquid–liquid interface serves as an ideal synthetic template, enabling superior control over the assembly, and templated growth of self-supported LDH tubes under RD conditions. Furthermore, we demonstrate that the adoption of this concentric fluid stream configuration also enables an "on-the-fly" formation of LDH-based composite structures that can be directly integrated into a device for characterization and function analysis. Specifically, we demonstrate the successful generation of millimeter-scale LDH@carbon nanotubes (CNTs) hollow structures, exhibiting similar morphology, and size to the bare LDH hollow structures produced with the same concentric liquid–liquid interface approach. The developed LDH@CNTs composite structures display electrical transport properties, highlighting the potential of our methodology as a viable solution for the direct integration of LDHs, and LDH-based composites into various devices. Note that the successful direct integration of millimetre scale LDH-based structures presents exciting opportunities for advancing performance and functionality in a range of applications, including sensing or energy storage, and conversion.

2. Results and Discussion

The formation of LDH hollow structures relies on the precise control of the reactant mixing at the concentric liquid–liquid

J. Puigmartí-Luis
Institució Catalana de Recerca i Estudis Avançats (ICREA)
Pg. Lluís Companys 23, Barcelona 08010, Spain

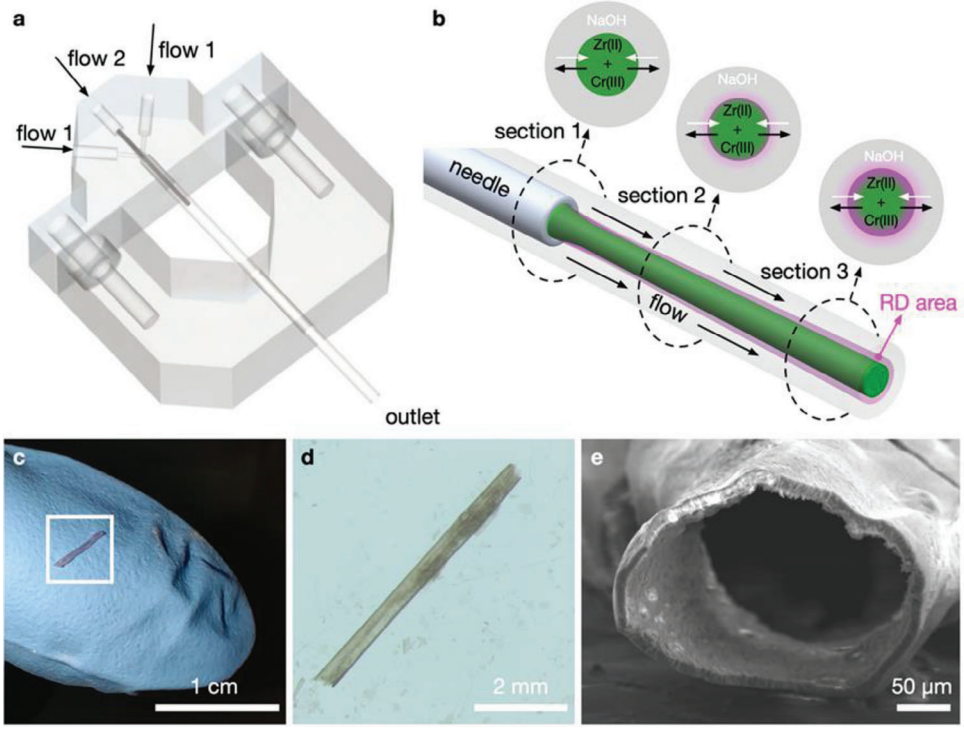

Figure 1. Schematic illustrations showing both, the continuous flow microfluidic device (a), and the progressive development of the RD area, which occurs downstream along the main channel (b). Note that the RD area (shown in pink in Figure 1b) is strategically positioned at the concentric liquid-liquid interface. c,d) Micrographs of millimetric ZnCr LDH hollow fibers. e) SEM image of a ZnCr LDH hollow fiber showing its micrometric wall thickness along with the distinctive hollow interior.

interface that we achieve by using a continuous 3D hydrodynamic flow focusing device, comprising a linear reaction channel (main channel) and three inlet ports (**Figure** 1a). The main channel consists of a microfluidic tubing with a cross-section (inner) diameter of 1 mm and length of 10 cm, opportunely hold in place by a 3D printed plastic holder (see the supporting information (SI) for further details). Note that the solution injected through the central inlet (Flow 2 in Figure 1a) remains surrounded and focused in the center of the main channel by a concentric sheath created by the solutions injected through the lateral inlets (Flow 1 in Figure 1a). When operating this microfluidic device, two important parameters must be taken into account: i) the total flow rate (TFR), i.e., the sum of the flow rates of the solutions injected into the three inlets, which determines the total residence time of the reactants in the device; and ii) the flow rate ratio (FRR), defined as the ratio of the sheath flows to the central inlet flow, which determines the diameter of the concentric RD area generated between the sheath and central inlet flows, shown in pink in Figure 1b. To characterize the hydrodynamic properties of our microfluidic device, while directly visualizing the effect of the

FRR on the hydrodynamic flow focusing, we performed preliminary experiments using a blue food dye (Figure S1, Supporting Information). In these experiments, the dye was introduced through the central inlet (i.e., Flow two inlet), while water was simultaneously injected through the two lateral inlets (i.e., the two Flow 1 inlets). This deliberate configuration led to the creation of a concentric liquid–liquid interface, effectively confining the blue dye-laden stream to the middle section of the main channel (Figure S1, Supporting Information). When the FRR was increased from 2 to 20, the hydrodynamic flow focusing clearly increased with an evident squeezing of the blue dye-laden stream. For example, we observed that at a distance of 1 mm from the microfluidic tubing's tip downstream of the primary channel, the cross-sectional area of the blue dye-laden stream decreased from ≈331 830 µm^2 at a FRR of two to roughly 25 446 µm^2 when the FRR was increased to 20. Notably, throughout this range of FRRs, the flow profile remained stable without any observed turbulence. To investigate the formation of LDHs using this continuous flow microfluidic device, we selected ZnCr LDH as our model system. This selection is based on the high stability of ZnCr LDH, and the growth behavior of Cr-based LDHs, which undergoes a single precipitation step at pH values higher than 5, making it a well suitable model system for synthesis control through modulation of microfluidic parameters (vide infra).

In a typical experiment, we injected an acidic solution (pH = 3) containing the two metal cations, Zn^{2+}, and Cr^{3+}, with a Zn/Cr ratio of 2:1, through the central inlet of the microfluidic device (i.e., through Flow 2). Simultaneously, an alkaline solution of NaOH (2 M) was injected through the lateral inlets (i.e., through Flow 1), serving as the precipitating agent for the reaction. Note that this experimental setup enables to establish the concentric liquid–liquid interface between the central laden stream transporting the metal cations and the alkaline sheath surrounding it. In addition, diffusion of the metal ions outward of the middle stream, and of NaOH toward the center of the main channel, creates well-defined concentration and pH gradients at each

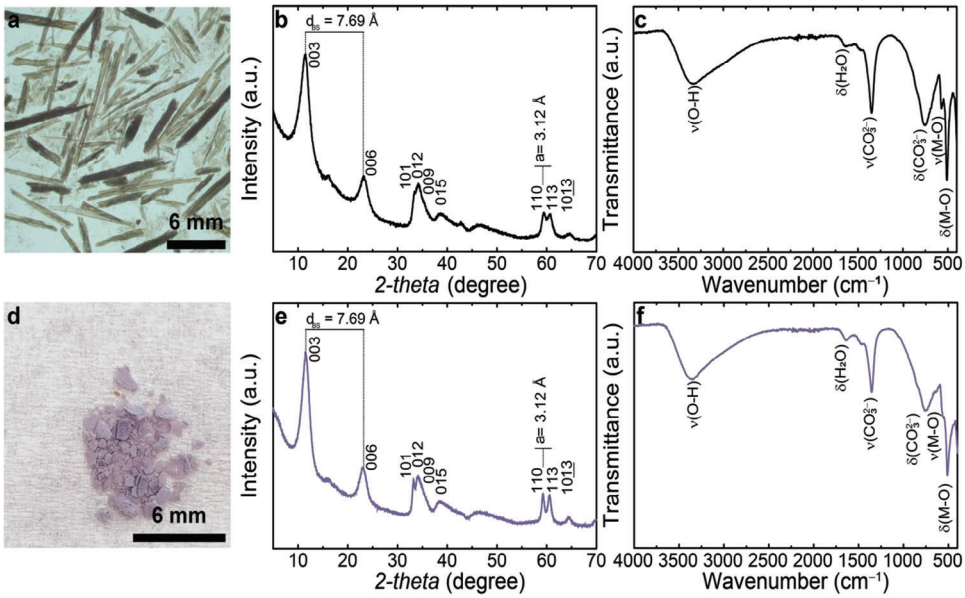

Figure 2. a) Optical microscope image of ZnCr LDH hollow structures. b) PXRD pattern, and c) FTIR–ATR spectrum of ZnCr LDH hollow structures. d) Micrograph of the ZnCr LDH powder produced in bulk under turbulent mixing. e) PXRD pattern and f) FTIR–ATR spectrum of the ZnCr LDH powder.

channel cross-section while the injected solutions move downstream the main channel (i.e., steady state gradients are being generated, see Figure 1b). Since under laminar flow conditions the mixing of reactants is solely mediated by a diffusion-limited process, the ZnCr LDH growth is confined to specific regions surrounding the concentric liquid–liquid interface where the cation concentration and pH reach optimal values for nucleation and subsequent growth of the ZnCr LDH material. In addition, the continuous injection of the solutions inside this microfluidic device ensures a continuous supply of precursors at the nucleation and growth region. This continuous supply prevents a depletion regime and enables a continuous synthesis. As a result, millimetre long self-supported hollow tubular structures are formed in ≈2 s (i.e., the residence time), and are collected directly at the outlet of the microfluidic device (Figures 1c,d and 2a). In order to find the best operating conditions for the synthesis of the self-supported hollow tubular structures, we screened the microfluidic parameters TFR (within the range 1050–4200 μL min^{-1}) and FRR (from 0.3 to 10), and we could identify combinations of values of these parameters that enable the formation of self-supported hollow structures (see Table S1, Supporting Information). For example, when the microfluidic synthesis was performed at TFR 2100 μL min^{-1} and FRR of 3 (see Supporting Information for further details), we could achieve the continuous formation of insoluble straight self-supported hollow structures, with a purple color and length of several millimeters, which could be easily washed and isolated, as shown in Figure 1c. Although the presence of an internal cavity was quite recognizable by optical microscopy (Figure 1d), it was unambiguously confirmed by scanning electron microscopy (SEM) as shown in Figure 1e. During the preparation of SEM samples, which involved depositing the hollow structures onto carbon tape followed by gold sputtering, we cracked opened some hollow structures to measure the wall thickness that were found to be in the order of tens of microns (see Table S1 and Figures S2 and S8, Supporting Information). The small wall thickness clearly suggests that the reaction/precipitation occurs in a very narrow and localized zone within the concentric liquid–liquid interface. Interestingly, the external surface of self-supported hollow structures (grown in contact with the alkaline solution) appears to be smoother than the inner surface (Figure S2, Supporting Information). This observation was further confirmed performing high magnification SEM images of the inner and outer surface of different ZnCr-LDH hollow structures (see Figures S3 and S4, Supporting Information). Additionally, high resolution TEM (HRTEM) studies revealed the presence of domains possessing different orientation but regular spacing (see Figure S5, Supporting Information). The absence of preferential orientation was also observed via polarized optical microscopy and Mueller matrix measurements, as shown in Figures S6 and S7 (Supporting Information).

The elemental composition analysis, performed using energy dispersive X-ray spectroscopy (EDS) confirmed the presence of both metals (Zn^{2+} and Cr^{3+}) in the expected 2:1 theoretical ratio, as well as of oxygen, as shown in Figure S9 and Table S2 (Supporting Information).

Note that this control over the size and shape of self-supported hollow structures cannot be achieved with conventional synthetic approaches. For the sake of comparison, we also did the reaction using a conventional co-precipitation method. This involved a bulk mixing of the acidic solution containing the metal cations with a NaOH solution. Namely, we used the same precursor solutions as the ones injected in the microfluidic device. To facilitate a rapid and turbulent mixing of the reagents, we employed vigorous vortex stirring. Subsequently, the reaction mixture was left at room temperature for a duration of 2 h, leading to the precipitation of a purple powder (Figure 2d) containing both metals in the expected 2:1 ratio, as confirmed by EDS (Figure S10 and Table S2, Supporting Information). Moreover, SEM images of the obtained product showed a heterogeneous morphology of the solid powder, demonstrating that the conventional synthetic approach did

not provide any control over the size or shape of the obtained material, as shown in Figure S11 (Supporting Information).

To unequivocally confirm the ZnCr LDH nature of both the self-supported hollow structures and the bulk powder, we performed powder X-ray diffraction (PXRD) measurements. The corresponding PXRD diffraction patterns are shown in Figure 2b,e, respectively, revealing coincident reflections at 11.5, 23.0, 34.0, 38.5, 42.8, 59.4, 60.6, and 64.8°. These patterns exhibit excellent agreement with the diffraction pattern previously reported for the hydrotalcite-like structure of ZnCr LDH, confirming the formation of the desired crystalline material.[28] Specifically, the basal space distance (d_{BS}) and intralayer parameter (a) are in perfect agreement with the ZnCr LDH phase.[29] Further, the Fourier transform infrared spectra attenuated total reflectance (FTIR–ATR) of both the self-supported hollow structures and bulk material (Figure 2c,f respectively) display vibrations at 3280 cm^{-1}, corresponding to the —OH stretching, at 650 and 500 cm^{-1}, associated with the M—O bonds, as well as bands at 1350 and 750 cm^{-1}, indicating the presence of carbonate (CO_3^{2-}) as the intercalating anion.[30] In fact, the use of a strongly alkaline solution for the synthesis of the ZnCr LDH (both in microfluidic and bulk conditions) favors the capture and solubilization of atmospheric carbon dioxide, which is thus present as intercalant in the LDH structure (as carbonate ion CO_3^{2-}). Carbonate has a strong interaction with the hydroxide layer and quickly exchanges the counter anion from the precursors metal salts, namely Cl^-, in the LDH structure, as also in agreement with the basal space distance (d_{BS}) of 7.69 Å observed in the PXRD patterns.

To further showcase the versatility of our microfluidic approach, we decided to decrease the TFR during the fabrication of the self-supported ZnCr LDH hollow structures from 2100 to 1050 μL min^{-1} while keeping the FRR at 3. This deliberate modification was aimed at facilitating the enhanced diffusion of the two metal cations and alkaline solution along the main channel and toward the outlet. We sought to increase the diffusion of reactants inside the RD area (i.e., the reaction area) to facilitate the formation of non-hollow ZnCr LDH fibres. Remarkably, our observations revealed a consistent trend wherein exclusively non-hollow fibers were generated across the entire spectrum of conditions, ranging from a FRR of 2 to 10, while maintaining the TFR at 1050 μL min^{-1} (Table S1 and Figure S12, Supporting Information). As shown in Figure S13 (Supporting Information), the obtained PXRD data unequivocally confirmed that all the non-hollow fibers produced at a TFR of 1050 μL min^{-1} and FRR of 2, 3, or 10 are indeed composed of ZnCr LDH. Furthermore, when we increased the TFR beyond 2100 μL min^{-1} (e.g., to 4200 μL min^{-1}), we observed the formation of non-complete hollow structures. These results clearly indicate that at TFRs exceeding 2100 μL min^{-1} (i.e., for shorter residence times), the time available for the diffusion of reactants inside the concentric RD area is insufficient to achieve the closure (or complete assembly) of the hollow structures (Figure S14, Supporting Information). PXRD analysis confirmed that also these non-complete hollow structures are composed of ZnCr LDH (Figures S13, Supporting Information).

From an application perspective, LDHs are emerging as promising materials for a variety of electrochemical applications, including sensing, energy storage, and conversion.[31,32] Nevertheless, one main drawback in this field lies in the inherent insulating behavior of bare LDHs, which can be overcome by the generation of hybrid-materials in which LDHs are blended with a conductive carbon matrix.[33–36] Capitalizing on the capability to fabricate millimeter scale self-supported ZnCr LDHs hollow structures through our dynamic and concentric microfluidic-based liquid–liquid interface, we explored the possibility of preparing a self-supported ZnCr LDH@carbon nanotubes (CNTs) composite material utilizing the same one-pot microfluidic-based reaction process. Note that the synthesis of self-supported LDH-based materials with controlled hierarchical structuring at the millimeter scale using a simple one-pot reaction method has remained largely unexplored in the scientific community, however, there is a pressing need for the development of such technology to significantly enhance the performance, functionality, and seamless integration of LDH-based materials into ready-to-use devices.

To address this grand challenge, we made modifications to the microfluidic synthesis protocol used during the formation of self-supported ZnCr LDH hollow structures by introducing a dispersion of commercial CNTs (i.e., TUBALL-BATT-H2O) in addition to the NaOH solution through the lateral inlets (i.e., the two Flow 1 in Figure 1a). Similar to the previous synthesis, the two metal cations, Zn^{2+} and Cr^{3+} (with a Zn/Cr ratio of 2:1) were injected through the central inlet of the microfluidic device (see SI for further details for this synthetic procedure). Note that the CNT source used in our work has been commonly employed to create hybrid conductive composites with enhanced water solubility and stability, features that are achieved by using carboxymethyl cellulose as modifier agent in its formulation. Interestingly, we observed that the presence of suspended CNTs did not significantly affect the hydrodynamic stability of our reagent-laden flows. As a result, we could still achieve a continuous formation of hollow structures with lengths of several millimetres in ≈2 s, but in this case showing a darker color, along with black striations, and suggesting the incorporation of the carbon-based material (**Figure 3**a). Indeed, PXRD measurements confirmed the formation of the ZnCr LDH composite material, without noting any variation of the basal distance (Figure 3c), suggesting a localization of the CNTs outside the LDH crystalline domains, as also shown in the HRTEM image (Figure S15, Supporting Information). Additionally, the SEM images also verified the hollow structure of the self-supported ZnCr LDH@CNTs composite material, with a wall thickness comparable to that of the bare ZnCr LDH hollow structures (Figure 3b). The SEM analysis revealed that the CNTs were predominantly absorbed onto the external smooth surface of the ZnCr LDH@CNTs hollow structures, creating a distinctive network-like layer (Figures S16–S18, Supporting Information). To demonstrate the presence of CNTs in the ZnCr LDH@CNTs hollow structures, we employed confocal Raman microscopy. As shown in Figure 3f, the Raman spectra obtained clearly confirmed the presence of CNTs from the appearance of their characteristic bands located at ca. 1580 cm^{-1} (intense G band originated from the in-plane lattice vibrations) and at ca. 2650 cm^{-1} (second overtone of the G band). These Raman vibrations correspond to those measured for the CNTs coming from the precursor CNT solution. Conversely, bare ZnCr LDH hollow fibres do not show any Raman signal in this region of the spectra (data not shown). The Raman mapping of a single isolated ZnCr LDH@CNTs hollow structure at the intensity of the G band

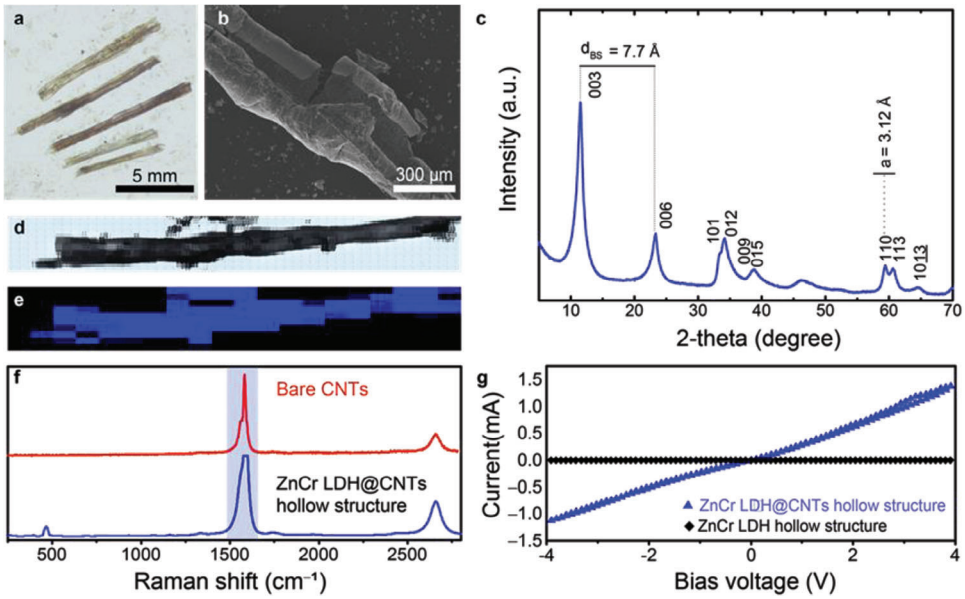

Figure 3. a) Optical microscope and b) SEM images of ZnCr LDH@CNTs hollow structures. c) PXRD pattern of the ZnCr LDH@CNTs hollow structures. d,e) Optical microscope and Raman map of a ZnCr LDH@CNTs hollow structure. The Raman map presented in (e) is acquired at 1580 cm^{-1} (i.e., at the G band of CNTs) highlighted in blue in (f). f) Raman spectra of CNTs (red) and ZnCr LDH@CNTs hollow structures (black). g) *I–V* sweeps of a ZnCr LDH hollow structure (blue) and a ZnCr LDH@CNTs hollow structure (black).

(i.e., at 1580 cm^{-1}) clearly demonstrated that the CNTs are uniformly spread all over the external area of the composite hollow structure (Figure 3d,e). Taken all together, these observations unequivocally confirm the successful formation of millimetre-long ZnCr LDH@CNTs hollow structures with our synthetic one-pot microfluidic approach and only requiring ≈2 s. Next, and taking advantage of the direct integration that can be accomplished with these millimetre-long ZnCr LDH@CNTs hollow structures, we prepared a two-point resistance-measuring device at the level of the single composite hollow structure to study its conductivity properties (Figures S19–S21, Supporting Information). As an internal reference, we used a bare ZnCr LDH hollow structure mounted nearby a ZnCr LDH@CNT hollow structure (Figures S20 and S21, Supporting Information). Upon applying a voltage across the two electrodes connected to the ZnCr LDH@CNTs hollow structure, we observed a distinct ohmic behavior in the acquired I/V sweeps, as reported in Figure 3g. Conversely, the bare ZnCr LDH hollow structure exhibited the anticipated insulating properties (Figure 3g). Based on these measurements, we were able to make a qualitative estimation of the equivalent resistance of the ZnCr LDH@CNTs hollow fiber, which falls in the kilo-ohm range (ca. 2,5 kΩ). In comparison to other LDH@carbon-based composite materials, this magnitude of resistance is high. Typically, LDH@carbon composites exhibit significantly lower resistance values, often ranging in milli-ohms or even micro-ohms.[37] However, it is important to note that these conductivity measurements for reported LDH@carbon-based composites are usually conducted after pelletization and densification methods, exclusively assessing the pressed composite materials devoid of any hierarchical control. Notably, in this study, we achieved a groundbreaking feat by successfully measuring a single self-supported ZnCr LDH@CNTs hollow structure without any post-processing (i.e., pelletization and densification) and after its direct integration into the measuring device. Moreover, the ZnCr LDH@CNTs hollow structure demonstrates robustness, as multiple measurements were conducted at high voltage values, such as up to 4 V, without any change observed in the I/V sweep measurements. This highlights the excellent durability and stability of the self-supported hollow composite structures fabricated with our home-made microfluidic approach.

3. Conclusion

In summary, our study demonstrates that redesigning the liquid-liquid interface in a continuous flow microfluidic device, transitioning from a vertical to a circular configuration, not only enables the generation of self-supported ZnCr LDH hollow structures in ≈2 s but it also facilitates the one-pot synthesis of conductive composites like the ZnCr LDH@CNTs hollow structures presented in this work. These results unequivocally demonstrate that the proposed technology is exceptionally well-suited for creating unprecedented self-supported hierarchical structures that can be directly integrated into functioning devices without the need for pelletization and/or densification approaches. Importantly, our method also eliminates the need for well-established multi-step and complex protocols like soft-templating methods or supported synthesis on 2D or 3D solid supports to achieve free-standing LDH structures at the millimeter scale. Furthermore, to highlight the versatility of our approach in generating self-supporting structures without relying on well-established multi-step and complex protocols, we have also synthesized unprecedented NiCo layered hydroxides (LH) hollow structures in their α phase in ≈2 s (see Figures S22,S23, Supporting Information). Note that α-NiCo LH is only generated under solvothermal conditions, and obtained in a powder form, after several hours of reaction.[38,39] Therefore, the ability to generate these

self-supported inorganic-based or composite structures at room temperature and in a significantly shorter time scale (i.e., seconds) opens up a new era of possibilities in materials engineering. We believe that our findings will inspire further research and innovation in the field of inorganic-based or composite LDH structures, pushing the boundaries of what can be achieved through continuous flow microfluidic devices and driving the scientific community toward exciting new frontiers in advanced materials design as well as in the fabrication of functional devices with targeted performances.

Supporting Information

Supporting Information is available from the Wiley Online Library or from the author.

Acknowledgements

This work was supported by the Swiss National Science Foundation (project no. 200021_181988, IZLCZ0_206033) and grant PID2020-116612RB-C33 funded by the MCIN/AEI/10.13039/501100011033. S.P. and J.P.-L. also acknowledge support from the European Union's Horizon Europe Research and Innovation Programme under the EVA project (GA No: 101047081). J.P.-L. acknowledges the Agencia Estatal de Investigación (AEI) for the María de Maeztu, project no. CEX2021-001202-M. Additionally, G.A. also acknowledges the European Research Council (ERC Starting Grant 2D PnictoChem No. 804110 and the ERC Proof of Concept Grant 2D4H2 No. 101101079), the Spanish MICIN (Projects PID2019-111742GA-I00, the Unit of Excellence "Maria de Maeztu" CEX2019-000919-M and TED2021-131347B-I00) and the Generalitat Valenciana (CIDEGENT/2018/001). V.O. also thanks ALN's membership.

Conflict of Interest

The authors declare no conflict of interest.

Data Availability Statement

The data that support the findings of this study are available from the corresponding author upon reasonable request.

Keywords

continuous flow microfluidic technologies, controlled diffusion, layered double hydroxides, material processing, self-standing hollow structures

Received: August 31, 2023
Revised: November 24, 2023
Published online: December 19, 2023

[1] A. Vaccari, *Appl. Clay Sci.* **2002**, *22*, 75.
[2] Q. Wang, D. O'hare, *Chem. Rev.* **2012**, *112*, 4124.
[3] S. He, Z. An, M. Wei, D G. Evans, X. Duan, *Chem. Commun.* **2013**, *49*, 5912.
[4] G. Mishra, B. Dash, S. Pandey, *Appl. Clay Sci.* **2018**, *153*, 172.
[5] C. Taviot-Guého, V. Prévot, C. Forano, G. Renaudin, C. Mousty, F. Leroux, *Adv. Funct. Mater.* **2018**, *28*, 1703868.
[6] G. Abellán, C. Martí-Gastaldo, A. Ribera, E. Coronado, *Acc. Chem. Res.* **2015**, *48*, 1601.
[7] J A. Carrasco, V. Oestreicher, A S-Da Silva, G. Abellán, *Appl. Clay Sci.* **2023**, *243*, 107073.
[8] S. He, J. Han, M. Shao, R. Liang, M. Wei, D. G. Evans, X. Duan, in *Handb. Solid State Chem*, Wiley-VCH Verlag GmbH & Co. KGaA, Weinheim, Germany, **2017**, pp. 541–569.
[9] Z. Zhang, G. Chen, *RSC Adv* **2014**, *4*, 31333.
[10] T. Hibino, *Eur. J. Inorg. Chem.* **2018**, *2018*, 722.
[11] J. Kameliya, A. Verma, P. Dutta, C. Arora, S. Vyas, R S. Varma, *Inorganics* **2023**, *11*, 121.
[12] R. Rojas, C E. Giacomelli, *Colloids Surf., A* **2013**, *419*, 166.
[13] Z. P. Xu, J. Zhang, M O. Adebajo, H. Zhang, C. Zhou, *Appl. Clay Sci.* **2011**, *53*, 139.
[14] A. U. Kura, M. Z. Hussein, S. Fakurazi, P. Arulselvan, *Chem. Cent. J.* **2014**, *8*, 47.
[15] S. Bullo, M. Z. Hussein, *Int. J. Nanomed.* **2015**, *2015*, 5609.
[16] Y. Sun, J. Zhou, W. Cai, R. Zhao, J. Yuan, *Appl. Surf. Sci.* **2015**, *349*, 897.
[17] Y. Tokudome, N. Tarutani, K. Nakanishi, M. Takahashi, *J. Mater. Chem. A* **2013**, *1*, 7702.
[18] Y. Tokudome, V. Prevot, N. Tarutani, *Appl. Clay Sci.* **2023**, *243*, 107051.
[19] X. Zhao, M. Yang, J. Wang, D. Wang, *Chem* **2023**, *39*, 630.
[20] T. Sadeghi Rad, A. Khataee, S. Sadeghi Rad, S. Arefi-Oskoui, E. Gengec, M. Kobya, Y. Yoon, *Ultrason. Sonochem.* **2022**, *82*, 105875.
[21] S. Sevim, A. Sorrenti, C. Franco, S. Furukawa, S. Pané, A. J. Demello, J. Puigmartí-Luis, *Chem. Soc. Rev.* **2018**, *47*, 3788.
[22] J. Puigmartí-Luis, *Chem. Soc. Rev.* **2014**, *43*, 2253.
[23] J. Puigmarti-Luis, D. Schaffhauser, B R. Burg, P S. Dittrich, *Adv. Mater.* **2010**, *22*, 2255.
[24] M. Rubio-Martinez, I. Imaz, N. Domingo, A. Abrishamkar, T. S. Mayor, R M. Rossi, C. Carbonell, A J. Demello, D B. Amabilino, D. Maspoch, J. Puigmarti-Luis, *Adv. Mater.* **2016**, *28*, 8150.
[25] A. Abrishamkar, S. Suárez–García, S. Sevim, A. Sorrenti, R. Pons, S.-X. Liu, S. Decurtins, G. Aromí, D. Aguilà, S. Pané, A. J. DeMello, A. Rotaru, D. Ruiz–Molina, J. Puigmartí-Luis, *Appl. Mater. Today* **2020**, *20*, 100632.
[26] N. Calvo Galve, A. Abrishamkar, A. Sorrenti, L. Di Rienzo, M. Satta, M. D'abramo, E. Coronado, A J. De Mello, G. Mínguez Espallargas, J. Puigmarti-Luis, *Angew. Chem., Int. Ed.* **2021**, *60*, 15920.
[27] D. Rodríguez-San-Miguel, A. Abrishamkar, J A. R. Navarro, R. Rodriguez-Trujillo, D B. Amabilino, R. Mas-Ballesté, F. Zamora, J. Puigmartí-Luis, *Chem. Commun.* **2016**, *52*, 9212.
[28] J W. Boclair, P S. Braterman, J. Jiang, S. Lou, F. Yarberry, *Chem. Mater.* **1999**, *11*, 303.
[29] C. Taviot-Guého, M. Halma, K. Charradi, C. Forano, C. Mousty, *New J. Chem.* **2011**, *35*, 1898.
[30] M. Del Arco, V. Rives, R. Trujillano, P. Malet, *J. Mater. Chem.* **1996**, *6*, 1419.
[31] N. Baig, M. Sajid, *Trends Environ. Anal. Chem.* **2017**, *16*, 1.
[32] M. Shao, R. Zhang, Z. Li, M. Wei, D G. Evans, X. Duan, *Chem. Commun.* **2015**, *51*, 15880.
[33] J. Zhao, J. Chen, S. Xu, M. Shao, Q. Zhang, F. Wei, J. Ma, M. Wei, D G. Evans, X. Duan, *Adv. Funct. Mater.* **2014**, *24*, 2938.
[34] C. Hou, T. Li, Z. Zhang, C. Chang, L. An, *Mater. Lett.* **2022**, *309*, 131361.
[35] C. Sun, Li Sun, K. Fan, Y. Shi, J. Gu, Y. Lin, J. Hu, Y. Zhang, *Dalt. Trans.* **2021**, *50*, 9283.
[36] L. Yang, D. Xu, H. Yang, X. Luo, H. Liang, *Chem. Eng. J.* **2022**, *432*, 134436.
[37] M. Latorre-Sanchez, P. Atienzar, G. Abellán, M. Puche, V. Fornés, A. Ribera, H. García, *Carbon N Y* **2012**, *50*, 518.
[38] D. Hunt, V. Oestreicher, M. Mizrahi, F G. Requejo, M. Jobbágy, *Chem. - Eur. J.* **2020**, *26*, 17081.
[39] N. Arencibia, V. Oestreicher, F A. Viva, M. Jobbágy, *RSC Adv.* **2017**, *7*, 5595.